



Design and analysis of a plasmonic split rings metasurface using characteristic mode theory for optical sensing

Atefeh Gholami¹ · Javad Ahmadi-Shokouh¹ · Hamideh Dashti¹

Received: 18 October 2021 / Accepted: 21 May 2022 / Published online: 22 June 2022
© The Author(s), under exclusive licence to Springer Science+Business Media, LLC, part of Springer Nature 2022

Abstract

In this paper, a plasmonic metasurface is proposed and designed that has switching capability and it can be used as a quantum switch as well as an optical sensor. To provide the switching characteristic, Kerr material is used with dimer split ring resonator. The Kerr material is considered to change the response from Fano to Lorentzian shape, thus two logical values of $|0\rangle$ and $|1\rangle$ can be made at the Fano dip resonance. The Characteristic Mode Theory is investigated to predict the occurrence of the Fano response with exact wavelength. The study shows that Fano response appears when the phase of CMT modes is around 90° . As a result, the Kerr material can impact the phase of CMT modes, that makes switching characteristic for the proposed metasurface, by reducing the phase value to 40° for various Kerr material implementation in the metasurface. Also in this paper, using eigenvalues, the exact location of the Fano response, was obtained and bright and dark modes are detected without plotting characteristic currents. The proposed metasurface is developed for optical sensing with high sensitivity as a part of optical and quantum spectroscopy. The sensitivity of the sensor is obtained around 400 nm/RIU which is sufficient to distinguish the materials and to have high resolution.

Keywords Fano · Plasmonic metasurface · Characteristic mode theory, Kerr material

1 Introduction

Plasmonics, is an interesting field for nano-optics and nanophotonics technology that aims to use the interaction of light and matter through the resonances of surface plasmons (Jiang et al. 2017). Surface plasmons (SP) have very attractive optical properties, such as the ability to restrict light in nanoscale and high sensitivity to the surrounding environment (Barbillon 2019). This capability has three major advantages: higher operating speed, smaller devices and lower power consumption (Kasani et al. 2019). Rapid advances in nanotechnology and plasmonics have made it easier to manipulate the light at the nanoscale.

✉ Javad Ahmadi-Shokouh
shokouh@ece.usb.ac.ir

¹ Barbillon Faculty of Electrical and Computer Engineering, University of Sistan and Baluchestan, Zahedan, Iran

Localized surface plasmon (LSP) is an optical phenomenon created by trapping light near metal nanoparticles that are smaller than the wavelength of the incident light. This phenomenon originates from the interaction of light and surface electrons in a conducting band (Petryayeva and Krull 2011). Metal nanostructures are critical to many applications in the field of photonics, including biosensing (Mejía-Salazar and Oliveira Jr. 2018), nanolasing (Azzam et al. 2020), nonlinear optical processes (Panoiu et al. 2018), spectroscopy (Eschimese et al. 2019) and metasurface technologies (Bin-Alam et al. 2021). Among these structures, optical metasurfaces have been noticed for precise light wave control and integrated quantum technology (Georgi et al. 2019). These metasurfaces are 2D surfaces based on the array of meta-atoms or optical nano-antennas. Metasurfaces are beneficial in fabrication which is usually made by replacing bulky optical components with ultra-narrow planar elements (Jha et al. 2017). These structures can manipulate the phase, amplitude and local polarization of the electromagnetic field (Zhou et al. 2020).

Among all Plasmonic structures, the Plasmonic nanoantenna play an important role in nanophotonics due to the enhancement intensity of the electromagnetic field that is controlled in general with coupling modes for Fano resonance (Butet and Martin 2014). In some ring-like structures, the coupling of nanoparticles is considered to confine and manipulate light (Zarrabi and Moghadasi 2017). Coupling between Plasmonic nanostructures is a simple and fast way to generate the Fano response (Wang 2018). These kind of resonance are seen in various structures including the symmetry breaking ring cavity (Lin et al. 2019), metal–insulator–metal waveguide (Wang et al. 2019), self-assembly of magnetic–Plasmonic core–shell nanoparticles (Liu et al. 2016), and plasmonic device consisting of a gold nanoparticle between two electrodes (Vardi et al. 2016). Fano resonance has significant applications in sensors due to its asymmetric and sharp spectral shape and strong field enhancement (Tavakoli et al. 2019). These type of sensors show great applications in the areas of biomedical diagnostics (King et al. 2015), healthcare (Shrivastav et al. 2021), environmental monitoring (Zhan et al. 2015), homeland security (Saylan et al. 2020) and chemical reactions (Stockman 2015).

On the other hand, numerous theoretical, computational and numerical simulation tools have been developed in recent years to understand the optical properties of plasmonic structures. One of the methods, that has recently shown its ability to analyze the intrinsic properties of plasmonic structures, is the Characteristic Mode Theory (CMT) (Ylä-Oijala et al. 2017), (Dey et al. 2019). CMT is a powerful tool based on the numerical Method of Moment (MoM) that allows the study of the intrinsic properties of a structure such as the resonance frequency of modes, the ability to couple each mode with an external field, the bandwidth of modes and the distribution of characteristic currents by solving the integral equations of electric and magnetic fields (Chen and Wang 2015).

A metasurface has been proposed using a Kerr material that has created significant coupling and controllability between modes, which without the use of this type of material, either this amount of coupling does not appear or is possible by creating much small inter-particle distances. That is a challenge in the manufacturing process. Moreover, the switching ability of the proposed metasurface at the Fano dip wavelengths makes this metasurface suitable for quantum computing. Finally, this metasurface is exerted as a plasmonic sensor and the results show that this sensor is more sensitive than previous structures. CMT is exploited to analyze the optical properties of the structure and it reveals the relation between the phase of the characteristic modes and Fano resonance. This method justifies how these arrangements affect the modes and the frequency of dark and bright modes with Fano dip. It also gives a glimpse of what happened in the far-field, using the distribution of characteristic currents and near-field results. Also, using the eigenvalues obtained

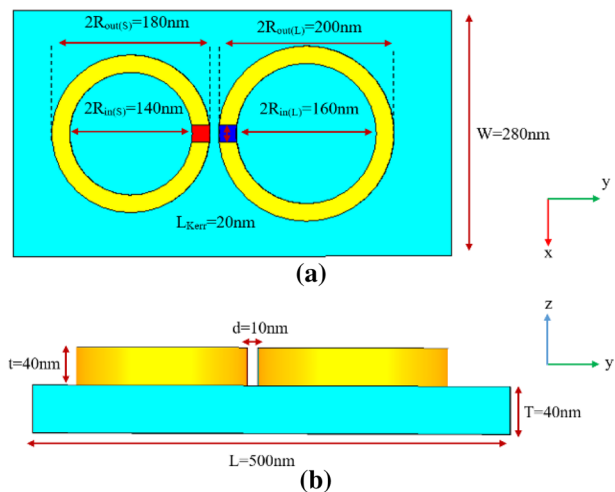
from CMT, the exact location of the Fano response and the modes causing this type of coupling are predicted, which had been obtained approximately, before in (Gholami 2021). Also, dark and bright modes are specified without the need to draw characteristic currents. So, CMT can be used as a tool to control the Fano response for specific purposes by plasmonics researchers.

2 Metasurface design and simulation

2.1 Introducing the structure and analysis methods

Due to the high intrinsic symmetry of the ring-like property, these structures are used for manipulating the light in a small volume. The metal rings are explored for plasmon resonances for the proposed metasurfaces and, besides, its fabrication with conventional lithography has led to the use of such structures in applications beyond chemical and biological sensing (Nordlander 2009). Based on the aforementioned advantages, the parallel rings nanoparticles are investigated as a plasmonic metasurface for switching and optical sensing in this study. Figure 1 shows a unit-cell of plasmonic metasurface studied from the top (Fig. 1a) and side (Fig. 1b) views. This metasurface consists of two rings with different diameters which are located on the SiO_2 substrate with the refractive index of 1.54 at the proposed spectrum. The outer radius of the larger ring is $R_{\text{out}(L)} = 100$ nm and the inner radius is assumed $R_{\text{in}(L)} = 80$ nm. These parameters are $R_{\text{out}(S)} = 90$ nm and $R_{\text{in}(S)} = 70$ nm for the smaller ring. For both rings, the thickness of the rings is assumed $t = 40$ nm. The edge-to-edge distance between the two rings is defined as $d = 10$ nm and the unit cell's substrate dimensions are $500 \times 280 \times 40$ nm³. Each ring has a gap of length, $L_{\text{Kerr}} = 20$ nm, which is filled with the Kerr material. This unit-cell is pinpointed on the X–Y plane and it is excited by a plane wave with x polarization and propagation direction in the z-direction. FEKO and CST software packages are used for simulation with two different techniques namely: MoM and finite integration technique (FIT), respectively. In this study, the nanorings are made of gold (Au) as the plasmonic material and Johnson & Christie's laboratory data are used for material

Fig. 1 Reconfigurable Kerr metasurface from **a** top and **b** side view



properties (Johnson and Christy 1972). The optical properties of a plasmonic structure in the far-field can be determined by the optical absorption, scattering, and extinction cross-section which can be described by (1):

$$C_{ext} = C_{abs} + C_{sca} \tag{1}$$

Since scattering and absorption both have significant values in the proposed metasurface, the optical extinction spectrum, which is the sum of these two effects, is presented as the optical response.

An in-house code is used for the characteristic mode analysis. In this way, the characteristic impedance matrix is extracted from FEKO, and after post-processing and using the equations in (Chen and Wang 2015), the modal significance (MS), characteristic angle diagrams, and characteristic current distribution are obtained. CMT in plasmonic material uses the PMCHW (Poggio–Miller–Chan–Harrington–Wu) formulas which are a set of coupled surface integral equations (Chen and Wang 2015). CMT forms a set of integral equations, using the principle of equivalence and definite boundary conditions, and creates some operator dependent on electric and magnetic fields. The generated integral equations are created and solved by MoM. The characteristic modes obtained from solving these equations, have the ability to describe the intrinsic properties of any structure, and they are independent of the excitation. In Fig. 2 it is brought a flowchart showing how to obtain the results of CMT. In the first step, the plasmonic structure is drawn in FEKO and triangularly meshed. The (.cfm) file, which contains the mesh information, is saved in this step. From this step onwards, in-house code is used. Using this code, (.pre) file of FEKO is opened for the structure drawn in the previous step, and the dielectric properties of the various materials are determined using it. To analyze the characteristic mode, we need the characteristic impedance matrix, which is obtained through MoM. CMT tool for plasmonic materials is not embedded in FEKO, but all analyzes in this software are using the Moment method. Therefore, it is possible to obtain a characteristic impedance matrix for plasmonic materials, although it is not possible to analyze the characteristic mode with this software. Therefore, in the third step, the characteristic impedance matrix for the desired structure is obtained which is stored in (.mat) file. This matrix is defined by (2), and extracted directly from FEKO:

$$\begin{bmatrix} Z^{EJ} & Z^{EM} \\ Z^{HJ} & Z^{HM} \end{bmatrix} \begin{bmatrix} J \\ M \end{bmatrix} = \begin{bmatrix} V^E \\ V^H \end{bmatrix} \tag{2}$$

where Z^{EJ} , Z^{EM} , Z^{HJ} and Z^{HM} are $N \times N$ matrices, (N is the number of common edges between two triangles, in the triangular meshing of the structure), that form the characteristic impedance matrix through the (3):

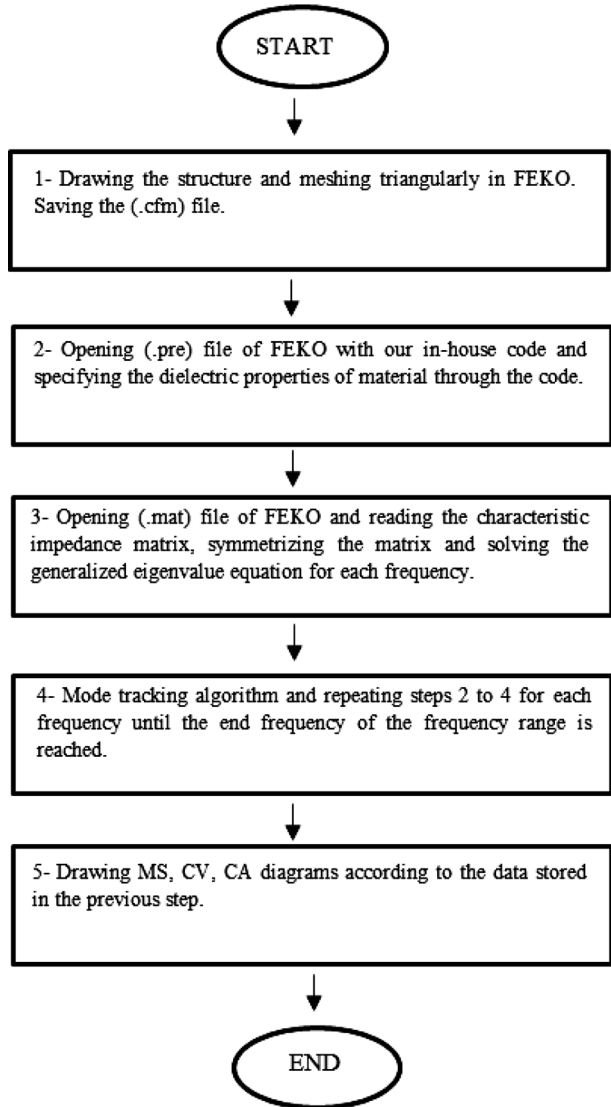
$$Z = Z^{EJ} - Z^{EM} (Z^{HM})^{-1} Z^{HJ} \tag{3}$$

Using (3), the characteristic impedance matrix becomes symmetric, which is necessary for CMT. By separating the real and imaginary parts of Z (R and X), the generalized eigenvalue equation is obtained by (4):

$$XJ_n = \lambda_n R J_n \tag{4}$$

λ_n is the eigenvalue and J_n is known as the eigenvector or eigencurrent.

Fig. 2 CMT computation flowchart



By obtaining this eigenvalue equation, it is possible to use the CMT equations and obtain the intrinsic properties of the radiator (Chen and Wang 2015). The above calculations are performed on single frequencies. To analyze the optical response of a structure, it is necessary to perform the analyzes in a frequency range. Therefore, in the fourth step, the mode tracking algorithm is used so that the modes that have the same index in different frequencies are known as one mode. The method we have used for mode tracking, is based on the orthogonality of the characteristic currents, that is (5):

$$r = \langle J_m^\dagger|_{f_1}, (RJ_n)|_{f_2} \rangle \approx \delta_{mn} \quad (5)$$

So that eigenvalues at frequency f_2 are correlated with eigenvalues at frequency f_1 . $J_{m,n}$ represent the characteristic currents and δ_{mn} is the Kronecker delta. Given that characteristic currents change very slowly during the frequency range, it can be expected to maintain their orthogonality in subsequent frequency iterations according to the above relation. When the modes have the same index, this value is very close to one, and if it is close to zero, the modes do not have the same index.

After applying the mode tracking algorithm and obtaining the modes in a frequency range, the characteristic mode parameters can be obtained in the whole frequency range, which is shown in the last step of the flowchart. For example, Modal Significance (MS) demonstrates the coupling ability of each characteristic mode with external sources and it is defined by (6):

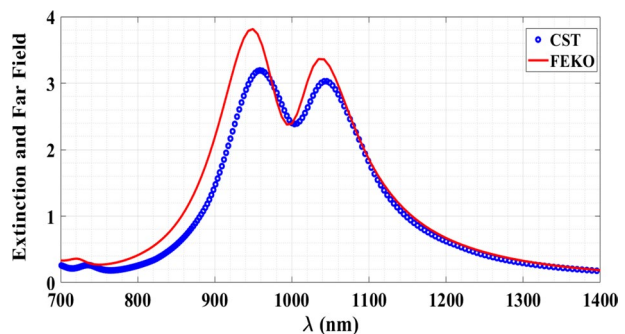
$$MS = \left| \frac{1}{1 + j\lambda_n} \right| \tag{6}$$

The modal excitation coefficient, which can be defined by $V_n = \langle E_{\tan}^i(r).J_n \rangle$, indicates the ability of coupling between the applied electric field and the n th eigenmode. Characteristic angle (CA) is another parameter used in CMT which offers a better representation of the behavior of each mode near the resonance frequency and it depends on eigenvalue or characteristic value (CV), by (7):

$$\alpha_n = 180^\circ - \tan^{-1} \lambda_n \tag{7}$$

The validity of this code is already shown in (Gholami et al. 2021), by comparing the results of two software, FEKO and CST. However, in order to compare the two different numerical methods, the optical response of the structure is presented in Fig. 3. The optical extinction spectrum and Far-field is obtained from CST and FEKO, respectively. For better comparison, the normalized to the maximum value is given. As shown in Fig. 3, this structure has two resonances (two local maximums), which can be seen in the results of both numerical methods. The slight difference in the resonance wavelength of the two software packages originates from the difference in numerical methods and the high sensitivity of the MoM to mesh density. Due to the similarities in the results, for analyzes other than CMT, the simulation results with CST are shown, in the continuation of this paper.

Fig. 3 Comparison of CST and FEKO results



2.2 Fabrication steps of the reconfigurable Kerr metasurface

The main steps of fabrication the metasurface are given in this section. The structure can be made on SiO_2 film, which is placed on a transparent material to prevent the structure from breaking. This material can be soda-lime glass, which is transparent at our operating frequency. Then, it is performed electron-beam lithography (EBL) on a resist polymethyl methacrylate (PMMA)-coated film, which is located on the substrate. Then, EBL-defined patterns should be removed by a methyl isobutyl ketone–isopropyl alcohol (MIBK–IPA) solution. For metal deposition step, the PMMA layer should be covered with 10-nm-thick titanium and 50-nm-thick gold. The lift-off process should be then performed to remove excess gold layers. Finally, plasma cleaning should be done to remove residual PMMA on the surface. By removing the extra layers, the final pattern is formed.

2.3 Study the Kerr material effect

As mentioned, reconfigurable materials can be implemented to design tunable plasmonic metasurfaces. Organic polymeric materials are of great interest due to their relatively low cost, ease of fabrication and integration in devices, higher laser damage threshold and fast nonlinear optical response. Here, polystyrene is exploited as a polymer and a reconfigurable material with a nonlinear Kerr effect that has the following optical parameters: a linear refractive index $n_0 = 1.59$ and a Kerr nonlinear coefficient $n_2 = 1.14 \times 10^{-12} \text{cm}^2/\text{W}$ that the latter coefficient depends on the third-order nonlinear susceptibility. Thus, the nonlinear refractive index can be obtained by $n_1 = n_0 + n_2 \times I$ where I is the local field intensity (Zhou et al. 2010). Due to the different values of I , the nonlinear refractive index of polystyrene takes on different values. In this paper, we have used polystyrene as a Kerr material with different refractive index based on the result obtained in (Zhou et al. 2010). Figure 4 shows the optical extinction spectrum of metasurface for two different polarizations. The gap in the larger ring is filled with Kerr material with a refractive index of 1.59 and the Kerr material used in the second ring changes and its refractive index varies from 1.59 to 2.4.

When the electric field has an X-direction and the refractive index of the material is 1.59 in both rings, two resonances are created at 958 nm and 1045 nm and a Fano dip at 1003 nm (blue diagram in Fig. 4a). This essentially means that the Fano dip has $|1\rangle$ value. By changing the Kerr material in the smaller ring to 1.7 (red diagram in Fig. 4a), the modes get closer and the coupling becomes more intense. So, the new resonances occur at 965 nm and 1042 nm. Similarly, as the Kerr material refractive index increases, the modes become closer and the coupling becomes more intense, such that for $n=2.4$, the Fano dip disappears and Lorentzian resonance is observed or, in other words, the value is $|0\rangle$ in this case. The proposed metasurface shows switching properties and by changing the Kerr material, switching occurs between the Fano response and the Lorentzian response and, ergo, this metasurface can be used for quantum computing or optical memory (Alexoudi et al. 2020). In the following, in order to further investigate the quantum application of the proposed metasurface, its function is described along with a figure (Fig. 5). In Fig. 5, it is shown an array of the original structure. Two sources are applied to the structure, which are referred to as pump and incident signals. The pump intensity determines the nonlinear refractive index of the Kerr material, which is I in the refractive index formula mentioned earlier. The incident wave is the source used to excite the structure. The pump signal sent by the

Fig. 4 The effect of changing Kerr material, for two different polarization **a** Electric field in X-direction, **b** Electric field in Y-direction

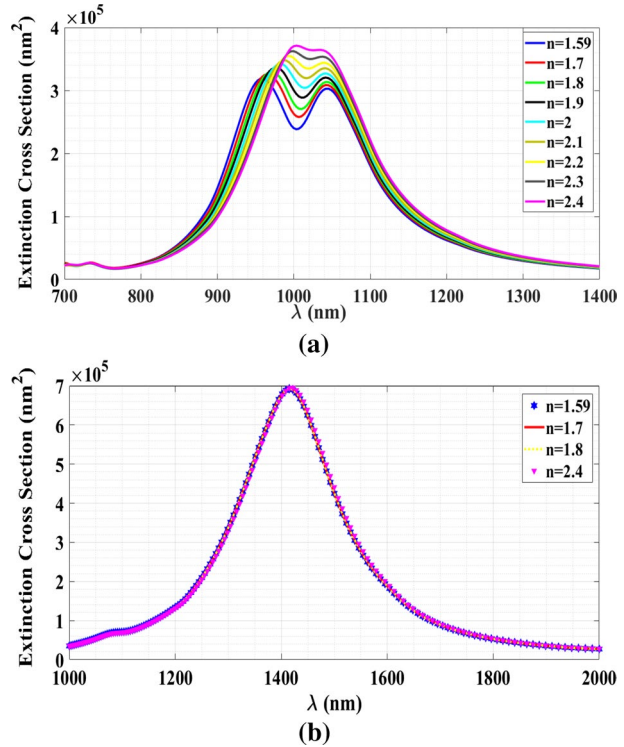
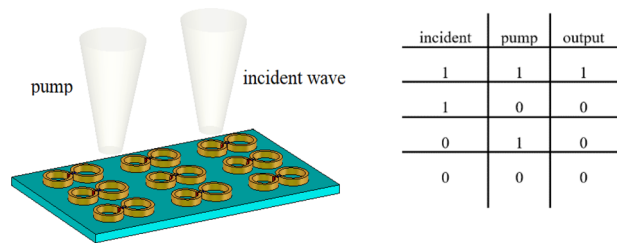


Fig. 5 The proposed metasurface with pump and incident signals



pump laser can be converted to photon through the setup given in (Wang et al. 2018) and used as a quantum source. The incident signal has a logic level of $|1\rangle$ until it is applied. The pump is disconnected and reconnected so that when there is a pump, the logic level is $|1\rangle$. The presence of a pump creates the same Kerr material in the gaps, creating a Fano dip, which is assumed to be a logic value of $|1\rangle$. By applying different pumps to the gaps, different refractive index can be created. The presence of the same or different Kerr materials, creates or eliminates the Fano and creates different logic levels. In fact, according to the pump, if the extinction rate of the structure at a wavelength of approximately 1000 nm is less than 3×10^5 , we have a Fano dip and a level of $|1\rangle$, otherwise a level of $|0\rangle$. So depending on the pump and the amount of extinction, we have a switching between the Fano and Lorentzian resonance. In fact, the presence of a pump creates a Fano dip, and this indicates the function of the structure as a quantum switch. This structure can also be used as a memristor (Ebrahimi et al. 2018), because if the input is $|1\rangle$, with the pump value of $|0\rangle$, the

output is $|0\rangle$, and if the pump is $|1\rangle$, the output is $|1\rangle$. If the input is $|0\rangle$, output with $|0\rangle$ value is generated with each pump signal. Now if several metasurfaces are used with different pumps, multi-bit gates can be produced that can be used in quantum computing.

Another noteworthy point is that by changing the Kerr material, a considerable coupling is observed such that if the Kerr material is not used in this structure, the distance between the rings must be much smaller than 10 nm to observe this amount of coupling. On the other hand, creating very small gaps between nanoparticles is a major challenge in the manufacturing process. As a matter of fact, gaps between elements should be greater than 10 nm for fabrication (Hatab et al. 2020), but by using different types of Kerr material, electrical distance can be reduced, which can be easily solved by using the Kerr material, as shown in Fig. 4a.

The effect of Kerr material changing for a Y-direction electric field is shown in Fig. 4b for comparing with the previous case in X-direction. In this case, the Kerr material has no effect on the optical extinction spectrum of the metasurface, and in all cases, a Lorentzian resonance occurs at 1422 nm. Therefore, by using the Kerr material and determining the appropriate polarization, a metasurface with switching capability can be designed. In short, by supposing a constant value of the refractive index for Kerr material, for example $n=1.59$, and by changing the incident wave polarization the value of the $|0\rangle$, X-polarization will change to $|1\rangle$ for Y-polarization at the Fano dip occurrence wavelength.

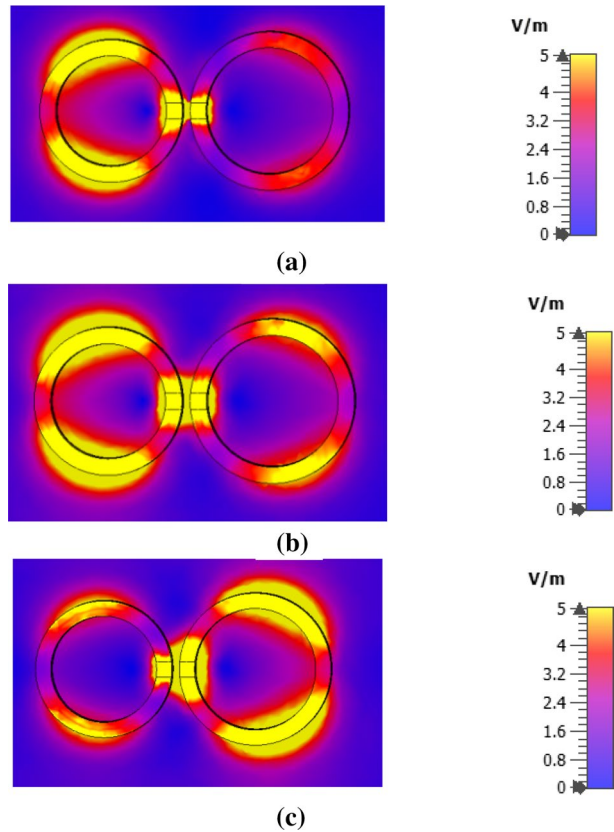
Figure 6 shows the near-field distributions of plasmonic metasurface at resonance wavelengths and the Fano dip for the case with the same Kerr material in both rings. In Fig. 6a, it has been shown that the first mode occurs at 958 nm, where the maximum field strength is around the smaller ring while the larger ring indicates a weakly localized field. The presence of a gap with the Kerr material in the rings has created higher-order modes. Also, according to the optical extinction spectrum in Fig. 4a, because this mode has more intensity, it forms a bright mode. Figure 6b shows the field distribution at the Fano dip wavelength. Very strong field is observed to be concentrated around the gaps. Moreover, the larger ring shows a stronger field than the first mode. In the second mode, at 1045 nm (Fig. 6c), the electric field is more concentrated around the larger ring, while the smaller ring shows a very weak field. According to the spectrum of optical extinction in Fig. 4a, because this mode is less intense, it forms a dark mode. Thus, the Fano resonance is created by dark and bright modes coupling.

The electric field distributions for different Kerr materials in gaps are studied and results are presented in Fig. 7 at three different wavelengths and it can be compared with the previous case. In this case, the Kerr material has a refractive index of 1.59 in the larger ring gap, while in the smaller ring, the refractive index of the Kerr material is 2.4. The dimensions of the rings are supposed the same as before. As shown in Fig. 7a, b, and c, at all three wavelengths, significant electric fields are concentrated near the nanorings and gaps, and they show the same behavior in terms of electric field distribution. This indicates more coupling of the modes and the approach of the Fano response to a Lorentzian response.

2.4 Characteristic mode analysis

As mentioned before, for characteristic mode analysis, the characteristic impedance matrix is needed, and FEKO is used for extracting the matrix based on MoM. After extracting this matrix from FEKO and creating the generalized eigenvalue equation, post-processing is performed and MS, characteristic angle, and characteristic currents are calculated. Figure 8 shows the MS and characteristic angle diagrams for the same Kerr material in gaps.

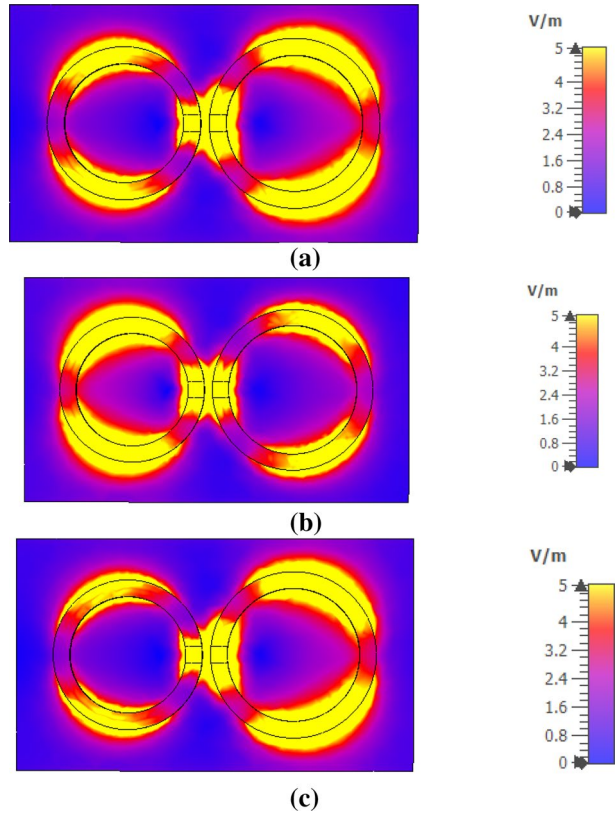
Fig. 6 Electric field distributions at wavelengths **a** 958 nm, **b** 1003 nm, and **c** 1045 nm for the same Kerr material



A common criterion in mode numbering, in CMT, is based on the smallest eigenvalue (largest MS) in the first frequency of the frequency band. Here, the same criterion is used to number the modes and to facilitate the comparison of the results, where all diagrams are driven based on the wavelength. The characteristic mode analysis of plasmonic metasurface with the same Kerr material (i.e., the same refractive index of 1.59 in the gaps of both rings) shows that this structure has 4 modes in the wavelength range of 700 nm to 1400 nm. The resonance wavelengths of these modes are at 1071 nm, 1027 nm, 950 nm, and 961 nm. These modes, are all modes that this structure can have in this wavelength range, which can be excited by different incident fields. In addition, as the dimensions of the nanoparticle are directly related to its resonance wavelength, it is expected that in lower wavelength modes, the smaller ring plays a major role and the larger ring is important for creating higher wavelength modes. As we know from CMT, at any frequency, the modes with $MS = 0.7$ or larger have resonance capability and they are called significance modes, while modes with $MS < 0.7$ have no resonance capability and they are called non-significance (Chen and Wang 2015).

According to Fig. 8a, modes 1 and 2 have resonances at 1027 nm and 950 nm, respectively, and their intersection has about $MS = 0.8$, so coupling conditions are provided, and their coupling creates a Fano resonance at about 990 nm. Moreover, mode 3 resonates in 1071 nm and can be a higher-order mode. The resonance wavelength of this mode is close

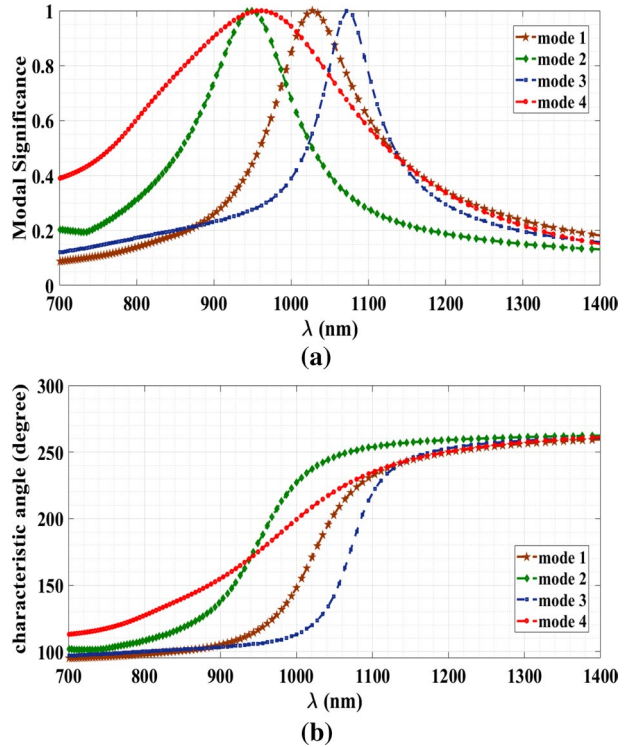
Fig. 7 Electric field distributions at wavelengths **a** 1003 nm, **b** 1024 nm, and **c** 1034 nm for different Kerr material



to mode 1, so it can merge the modes and eventually form a dark mode according to the optical extinction spectrum. Based on CMT, the modes resonate when their phase reaches 180° . Therefore, as shown in Fig. 8b, the phases of all modes are 180° at their resonance wavelength. Furthermore, the phase of mode 1 is about 130° and mode 2 is about 220° , at collision wavelengths of these modes at 990 nm. So, in Fano dip, the phase difference is about 90° . Therefore, the availability of modes coupling conditions, along with the phase difference of about 90° at the coupling wavelength, provide the conditions for creating a Fano response. So as a result, comparing to the scattering spectra in Fig. 4a, it is found that modes 1 and 2 are playing an important role in making the Fano response.

As shown in Fig. 8, the approximate location of the Fano response can be predicted using MS and characteristic angles diagrams. But when we are dealing with highly symmetrical structures, many degenerated modes appear as characteristic modes, and it will be difficult to identify the wavelength in which the Fano occurred according to the MS diagrams. The detection of the Fano response, according to the MS diagrams has been done before in (Gholami et al. 2021), but in that paper, the number of points of modes collision, was very high, so it is not possible to find the exact location of the Fano response according to the location of the collision of the modes, alone. Therefore, other criteria need to be considered to detect the Fano response. Since CMT, is an eigenvalues based method, eigenvalues of modes can be used as another criterion for determining the Fano response. It is shown in (Schab et al. 2016), that the eigenvalues of coupling modes are bending and

Fig. 8 **a** Modal Significance and **b** characteristic angle diagrams for plasmonic metasurface for the same Kerr materials



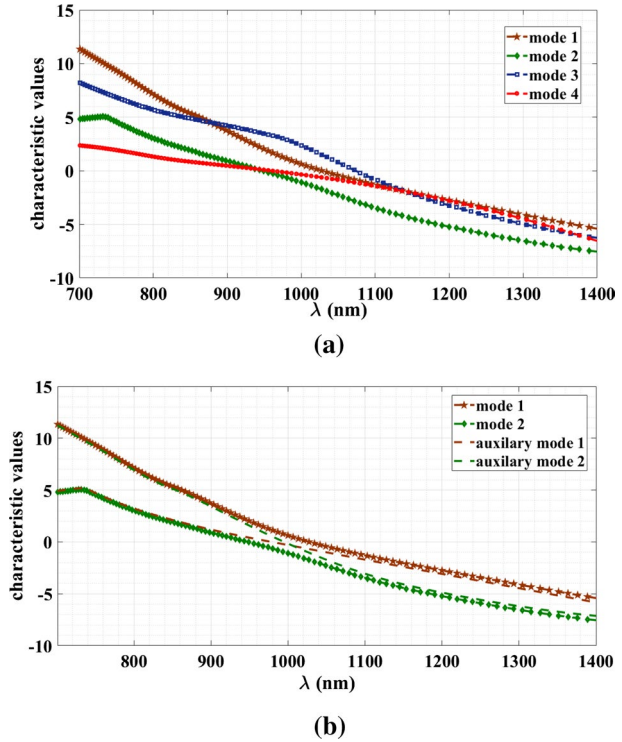
receding, but an intersection is shown in the eigenvalue diagrams for auxiliary modes. For this reason, the eigenvalues of plasmonic metasurface, is shown in Fig. 9. As shown in Fig. 9a, mode 1 is bended at a wavelength of about 990 nm and it is away from mode 2, while this bending is not in the face of modes 3 and also mode 4. Mode 2 has no intersection with mode 3, but according to Fig. 8a, in the intersection of these two modes MS=0.5, which is less than the required amount for coupling, therefore there are no coupling conditions. On the other hand, mode 2 intersects with mode 4, so coupling between these two modes cannot occur. Modes 3 and 4, also do not have this bending relative to each other, so it is not possible to couple these two modes. Therefore, modes 1 and 2 are the modes that created the Fano response, and the wavelength of the Fano dip, is at the bending point of these modes. In Fig. 9b, the eigenvalues for modes 1 and 2 and their auxiliary modes, are shown.

Auxiliary modes are uncoupled system modes and they are obtained through the following equations (Schab et al. 2016):

$$\lambda_a = \begin{cases} \lambda^m + d & f < f_0 \\ \lambda^m - d & f > f_0 \end{cases} \tag{8}$$

$$\lambda_a = \begin{cases} \lambda^m - d & f < f_0 \\ \lambda^m + d & f > f_0 \end{cases} \tag{9}$$

Fig. 9 **a** Eigenvalue diagrams for plasmonic metasurface modes, **b** eigenvalues of modes 1 and 2 and their auxiliary modes



where f_o is the frequency at which the modes bending, occurs, and λ_m is the eigenvalues average of the principal modes. G and d are obtained from the following equations (Schab et al. 2016):

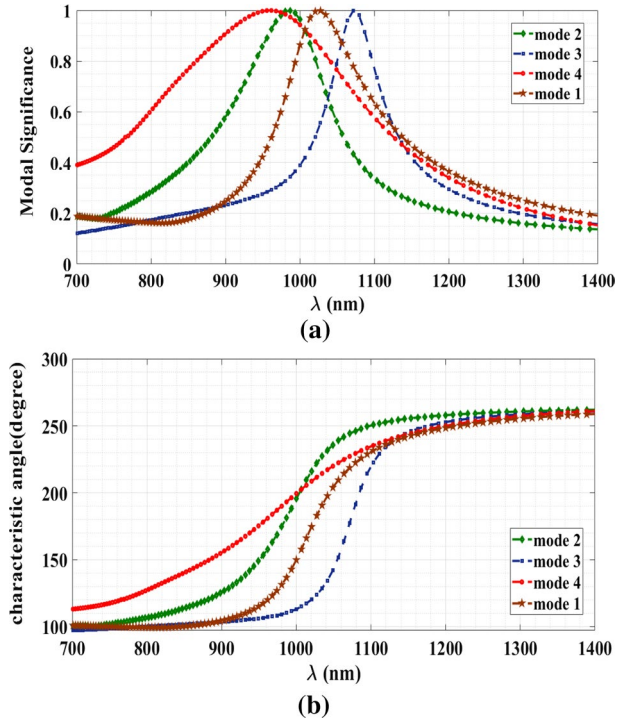
$$G = \min \{ |\lambda_1 - \lambda_2|/2 \} \tag{10}$$

$$d = \sqrt{\left(\frac{\lambda_1 - \lambda_2}{2}\right)^2 - G^2} \tag{11}$$

According to Fig. 9b, the auxiliary modes intersect at a wavelength of about 990 nm, where the bending of main modes, is created. Therefore, in order to determine whether the plasmonic structure has the ability to generate a Fano response or not, it is necessary to pay attention to the eigenvalues of the main and auxiliary modes in addition to the MS and characteristic angles diagrams. So, it is possible to determine the exact location of the Fano response.

The effect of Kerr material on the behavior of modes in CMT is investigated in Fig. 10, and the MS and characteristic angle diagrams are presented for the case when different Kerr materials are placed in gaps. As mentioned before, the refractive index of the Kerr material in a larger gap is 1.59 whilst it is 2.4 for the gaps in a smaller ring. The number of modes that are resonated in this wavelength range, is similar to the case where the same Kerr material is used in the gaps. The only difference in the results is the resonance wavelength of mode 2, shown in green, which now resonates at 987 nm. In this case, three

Fig. 10 **a** Modal Significance and **b** characteristic angle diagrams for plasmonic metasurface for different Kerr materials



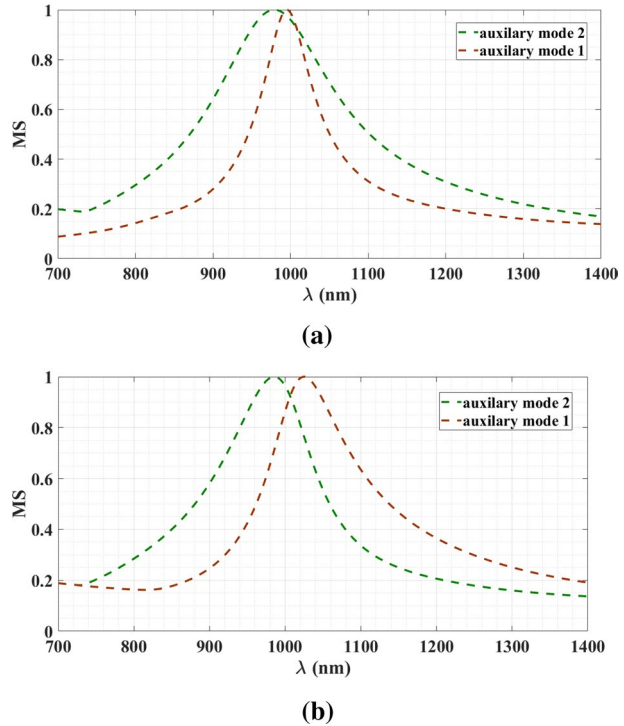
modes collide at 1007 nm. At the intersection of modes, it is observed that, $MS=0.9$, which is larger than what is shown in Fig. 8a. So, according to the definition of MS, a more intense coupling has occurred and the resonance wavelengths of modes are getting closer, which is also obtained by the optical extinction spectrum. In fact, the dark and bright modes are merging and removing the Fano dip. Furthermore, according to the phase diagram in Fig. 10b, the phase of mode 1 is about 160° and mode 2 is 200° , at the collision wavelength of modes at 1007 nm. Therefore, the phase difference of the modes has reached less than 45° , and in this case, the Fano response is converted to Lorentzian. Therefore, using CMT and the phase of the modes at their coupling wavelength, the occurrence of Fano resonance can be predicted.

Figure 11 shows the MS diagrams for auxiliary modes, given the following equations:

$$MS_a = \left| \frac{1}{1 + j\lambda_a} \right|, MS_b = \left| \frac{1}{1 + j\lambda_b} \right| \tag{12}$$

Figure 11a is for the case where the same Kerr material is used in the gaps of the rings, in which case we have already seen the Fano response. As shown in Fig. 11a, these two modes have different radiation bandwidth. Figure 11b also shows the MS for auxiliary modes in structures with different Kerr material in the gaps. The modes, in this case, have the same radiation bandwidth. On the other hand, according to the definition of the Fano response (Butet and Martin 2014), we know that the Fano response is due to the coupling of a bright wide mode with a narrow dark mode. Therefore, according to the MS diagrams, the presence of the Fano response in the first case and the lack

Fig. 11 MS diagrams for auxiliary modes, for **a** the same Kerr material in gaps and, **b** different Kerr material in gaps



of Fano formation in the second case can be observed. Also, it is possible to distinguish between bright and dark modes of the metasurface, which were previously only possible by drawing characteristic currents (Gholami et al. 2021).

In Fig. 8 the distribution of characteristic currents at wavelengths of 950 nm and 1027 nm, are given, corresponding to modes 2 and 1 in Fig. 12, respectively. The smaller ring has a higher current density at 950 nm (Fig. 12a), while in the larger ring the current is almost near to zero. Also, in the smaller ring gaps, the current intensity is very small, which is due to the low capacitance in this gap. These results are similar to the near-field distribution previously obtained (Fig. 6). In fact, at lower wavelengths, the smaller ring has the stronger field intensity and it is responsible for creating the first mode in the extinction spectrum. The current distribution shows that with the presence of a gap in the rings, the current distribution deviates from the dipolar state and takes the form of a higher-order mode, similar to what was previously observed in the near field distribution (Fig. 6a). Furthermore, a significant characteristic current is generated in the larger ring at 1027 nm (Fig. 12b), and due to the near-field distribution in Fig. 6c, the second mode in the extinction spectrum is created by this ring. The current of modes is matched with the scattering of the metasurface, so mode 2 is a bright mode and mode 1 is a dark mode.

Figure 13 shows the characteristic currents for cases with different Kerr materials. Similar to the previous case, the wavelength of 987 nm corresponds to modes 2, where the maximum characteristic current intensity happens in the smaller ring. Moreover, the characteristic current of the larger ring is predominant at 1027 nm. Also, by comparing the current distribution in the smaller ring gap in Fig. 13a with Fig. 12a, it can be said that the current intensity has increased due to an increase in the capacitance in the gap. Moreover,

Fig. 12 Characteristic current distributions of modes at **a** 950 nm, and **b** 1027 nm, for the same Kerr material in gaps.

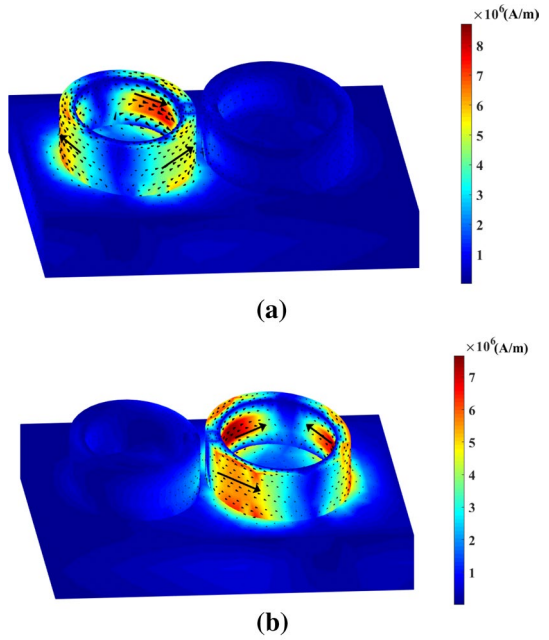
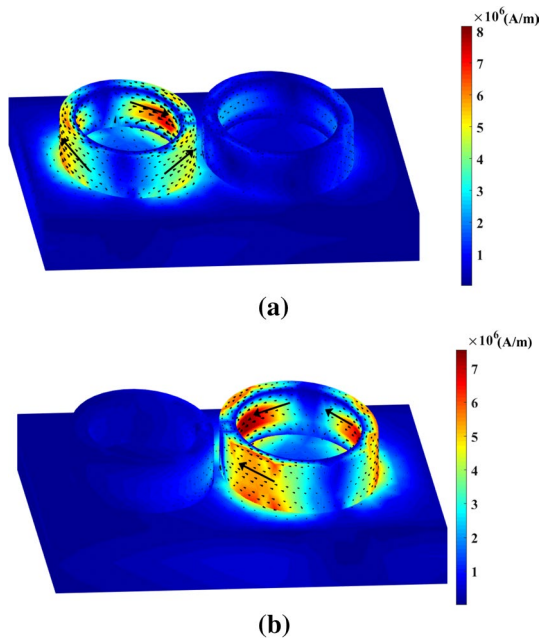


Fig. 13 Characteristic current distributions of modes at **a** 987 and, **b** 1027 nm, for different Kerr material in gaps.



by increasing the current density in one loop, the scattering diagram is more similar to the Lorentzian line shape.

2.5 The parametric study of plasmonic metasurface

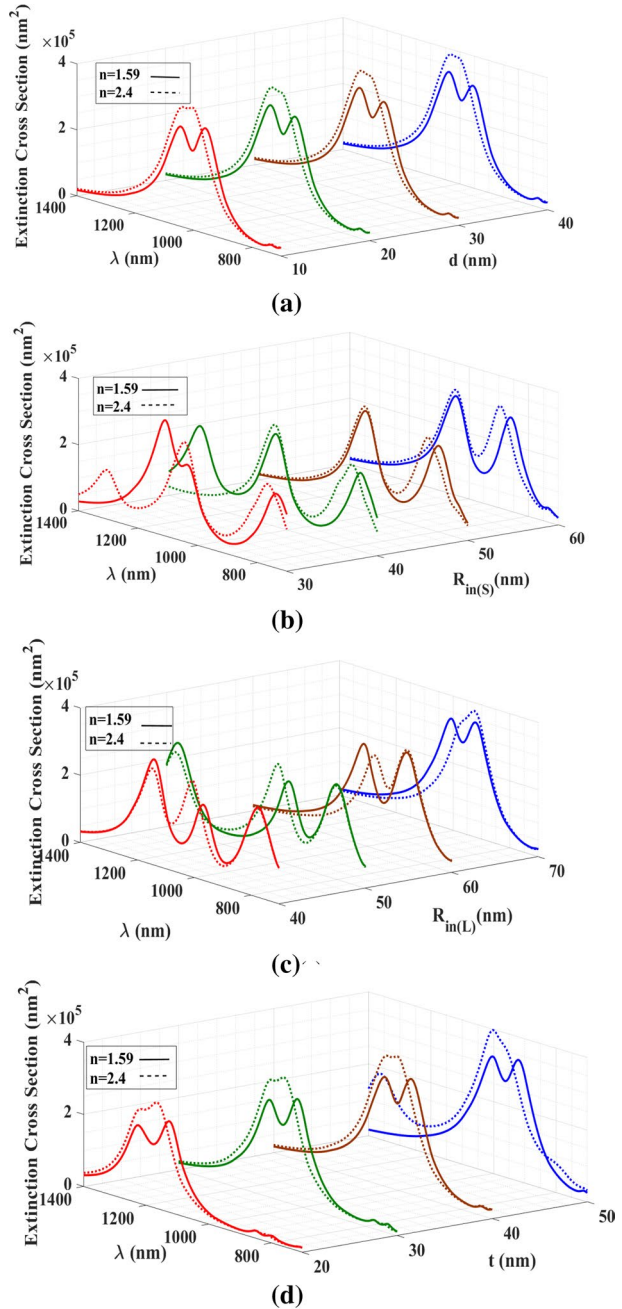
The effect of various parameters of the proposed structure, in controlling the switching effect is investigated, including the distance between the nanorings, the nanorings' thickness, and the radius of the inner core. In all figures, the line diagram corresponds to the same Kerr material with a refractive index of 1.59 in both gaps. The dashed line diagram corresponds to the different Kerr material with a refractive index of 1.59 in the larger ring gap, and a refractive index of 2.4 in the smaller ring gap. Figure 14a shows the effect of edge-to-edge distance of the rings for $d = 10$ nm, 20 nm, 30 nm, 40 nm. As shown in Fig. 14a, in all cases, when the same Kerr material is used in both gaps, two resonances are created and the Fano response is generated. The Fano dip is eliminated by changing the refractive index of the Kerr material in the smaller ring to 2.4, so a Lorentzian resonance is created.

In fact, despite the large distance of 40 nm between the nanorings, there is still a strong coupling between the modes, and switching has occurred. It is noteworthy that a very high coupling can be achieved using the Kerr material, even with a 40 nm distance between the nanorings. In Fig. 14b, the effect of changing the inner radius of the smaller ring on the optical extinction spectrum is investigated. The inner radius varies from 30 to 60 nm. At a smaller radius, more resonances are observed for both, same and different, Kerr materials. Increasing the inner radius reduces the number of resonances, and the resonant wavelengths are closer together and resulting in more intense coupling. The remarkable thing about all these diagrams is that when different Kerr material is used in the gaps, the resonance wavelengths get closer together. Also, as the radius increases, the shape of the spectrum gets closer to the Lorentzian response. Similar results are obtained for the larger ring in Fig. 14c. The inner radius of the ring varies from 40 to 70 nm. At a smaller radius, more resonances can be seen in the extinction spectrum. As the radius increases, the number of resonances decreases to two resonances. In this case, the use of different Kerr materials has increased the coupling and eliminated the Fano response. In fact, switching has occurred between the Fano and Lorentzian responses. Comparing with Fig. 14b, it is found that controlling the internal radius of the larger ring has a significant effect on the switching phenomenon in this structure. Finally, the effect of ring thickness is shown in Fig. 14d. The thickness of the rings varies from 20 to 50 nm. When the thickness is $t = 20$ nm (red diagram), the Fano response is seen in both cases. By increasing the thickness to 50 nm (blue diagram), the coupling of the modes becomes stronger so that, a completely Lorentzian resonance is observed for a different Kerr material.

3 Optical sensing performance

In this section, the performance of Metasurface as a sensor is examined and compared with similar structures. For this purpose, the metasurface and the dielectric substrate are covered by a layer with a thickness of 100 nm (inset in Fig. 15). The refractive index of the material changed from 1 to 1.2 with a step of 0.05. The presence of external material increases the capacitance of the metasurface, leading to a red-shift (shift to higher wavelengths) of resonance wavelength that occurs in both modes (Fig. 15). Sensitivity

Fig. 14 The effect of changing **a** the edge-to-edge distance of the rings, **b** the inner radius of the smaller ring ($R_{in(S)}$), **c** the inner radius of the larger ring ($R_{in(L)}$), and **d** the rings thickness



is obtained according to $S = \Delta\lambda/\Delta n$. The proposed metasurface shows a sensitivity of 360 (nm/RIU) in the first mode and a sensitivity of 400 (nm/RIU) in the second mode, which is a significant value for a Plasmonic sensor compared to similar structures in Table 1.

Fig. 15 Extinction spectrum at different refractive index of surrounding medium. The inset shows how the material under the test (MUT) is placed in the optical sensor

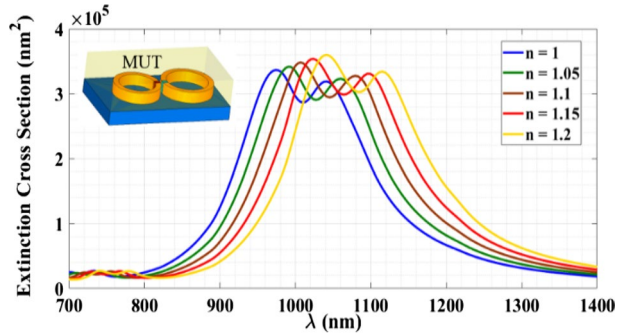


Table 1 Comparison of the proposed sensor with pervious study

	Type	Sensitivity (nm/RIU)	Wavelength (nm)
This work	Couples Ring	400	1003
Singh and Datta (2019)	Au Nanorings	66	1530
Wang (2018)	Coupled sphere	323–431	525–910
Figueiredo et al. (2020)	Nanocomposites	176	580
Martinsson et al. (2014)	Nanospheres	148	398
Martinsson et al. (2014)	Nanocubes	204	444
Martinsson et al. (2014)	Nanoplates	233	552

One of the uses of the plasmonic metasurface is to detect cancerous tissue in different parts of the body, such as the liver. Healthy and cancerous tissues have different dispersion relationships due to their different biological and chemical composites. The refractive index is an optical constant that plays an important role in describing the interactions of light and matter. The medium for analysis of the metasurface sensor is liver tissue samples. In (Giannios et al. 2016) the refractive index of healthy and cancerous human liver samples has been measured in the visible and near-infrared wavelength. Using the data in (Giannios et al. 2016), the complex refractive index of different liver tissues (normal or non-cancerous (N), metastatic (MET), and primary liver tumor (HCC)) is obtained from (13):

$$n_s = n_r + in_i \tag{13}$$

According to the values given at different wavelengths, the real and imaginary parts of the refractive index are obtained from the following equations:

$$n_r(\lambda) = A + \frac{B}{\lambda^2} + \frac{C}{\lambda^4} (\lambda : [\mu m]) \tag{14}$$

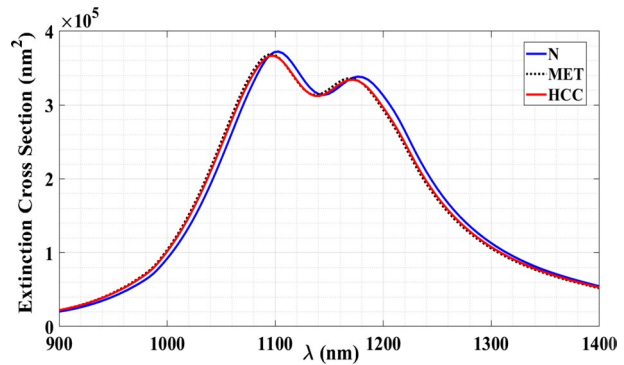
$$n_i(\lambda) = a.\lambda^{(1-b)} (\lambda : [nm]) \tag{15}$$

where the values of *A*, *B*, *C*, *a*, and *b* for different tissues are given in Table 2 (Giannios et al. 2016).

Figure 16 shows the optical extinction spectrum of metasurface for different liver tissues. As shown in Fig. 16, the proposed metasurface has the ability to identify healthy

Table 2 Fit parameters of various tissue groups

Tissue	Real index fit parameters			Imaginary index fit parameters	
	A	B(μm^2)	C(μm^2)	a	b
N	1.35910	0.00827	-0.000576	196	1.27
MET	1.34127	0.00634	-0.000324	780	1.41
HCC	1.34348	0.00998	-0.000793	145	1.14

Fig. 16 Extinction spectrum for different liver tissues

liver tissue from cancerous type, according to the corresponding refractive index values. The normal tissue extinction spectrum shows two resonances at 1103 nm and 1181 nm, while they occurred for malignant tissue, MET, at 1095 nm and 1167 nm, and for HCC at 1097 nm and 1172 nm, respectively. By the definition of sensitivity, and considering that according to the diagrams, the maximum wavelength shift is in the second mode, this metasurface shows the maximum sensitivity of about 1000 (nm/RIU) in the diagnosis of malignant liver tissues which is highly sensitive in the diagnosis of this cancer tissue.

4 Conclusion

In this paper, we have proposed a metasurface that, by using the Kerr material's capability, can overcome the challenges of creating short distances between nanoparticles, in the process of fabricating plasmonic and quantum structures. In addition, it has been shown that the proposed metasurface has the switching ability between Fano and Lorentzian response in Fano dip wavelength, which makes it suitable for quantum computing. CMT has been used to analyze the optical properties of the structure and we reveal the relation between the phase of the characteristic modes and appearing of the Fano resonance as well as the effect of the Kerr material on the frequency of dark and bright modes and Fano dip. We have also shown that, unlike previous studies that have shown the approximate location of the Fano response, the eigenvalues of CMT can be used to find the exact location of the Fano response and we can also distinguish between dark and bright modes, with the help of auxiliary modes, without needing to obtain characteristic currents. Finally, the performance of the proposed metasurface as an optical sensor has been investigated and it has

been shown that this sensor has a sensitivity of about 400 (nm/RIU) and it is able to distinguish healthy liver tissue from cancerous one with a sensitivity of 1000 (nm/RIU).

Funding The authors have not disclosed any funding.

Declarations

Conflict of interest The authors have not disclosed any competing interests.

References

- Alexoudi, T., Kanellos, G.T., Pleros, N.: Optical RAM and integrated optical memories: a survey. *Light Sci. Appl.* **9**(1), 1–16 (2020)
- Azzam, S.I., Kildishev, A.V., Ma, R.M., Ning, C.Z., Oulton, R., Shalae, V.M., Stockman, M.I., Xu, J.L., Zhang, X.: Ten years of spasers and plasmonic nanolasers. *Light Sci. Appl.* **9**(1), 1–21 (2020)
- Barbillon, G.: Plasmonics and its applications. *Materials* **12**(9), 1502 (2019)
- Bin-Alam, M.S., Reshef, O., Mamchur, Y., Alam, M.Z., Carlow, G., Upham, J., Sullivan, B.T., et al.: Ultra-high-Q resonances in plasmonic metasurfaces. *Nat. Commun.* **12**(1), 1–8 (2021)
- Butet, J., Martin, O.J.F.: Fano resonances in the nonlinear optical response of coupled plasmonic nanostructures. *Opt. Express* **22**(24), 29693–29707 (2014)
- Chen, Y., Wang, C.F.: *Characteristic Modes: Theory and Applications in Antenna Engineering*. John Wiley & Sons, Hoboken (2015)
- Dey, S., Chatterjee, D., Garboczi, E.J., Hassan, A.M.: Plasmonic nanoantenna optimization using characteristic mode analysis. *IEEE Trans. Antennas Propag.* **68**(1), 43–53 (2019)
- Ebrahimi, S., Sabbaghi-Nadooshan, R., Tavakoli, M.B.: DNA implementation for optical waveguide as a switchable transmission line and memristor. *Opt. Quant. Electron.* **50**(4), 1–13 (2018)
- Eschimese, D., Hsia, P., Vaurette, F., Deresmes, D., Bettignies, P.D., Schreiber, J., Chaigneau, M., Arscott, S., Lévêque, G., Mélin, T.: Comparative investigation of plasmonic properties between tunable nanoojects and metallized nanoprobe for optical spectroscopy. *J. Phys. Chem. C* **123**(46), 28392–28400 (2019)
- Figueiredo, N.M., Vaz, F., Cunha, L., Cavaleiro, A.: Au-WO₃ nanocomposite coatings for localized surface plasmon resonance sensing. *Materials* **13**(1), 246 (2020)
- Georgi, P., Massaro, M., Luo, K.H., Sain, B., Montaut, N., Herrmann, H., Weiss, T., Li, G., Silberhorn, C., Zentgraf, T.: Metasurface interferometry toward quantum sensors. *Light Sci. Appl.* **8**(1), 1–7 (2019)
- Gholami, A., Ahmadi-Shokouh, J., Dashti, H.: Analytical study of Fano phenomenon in plasmonic hexamer and heptamer using characteristic mode theory. *Optik* **243**, 11–13 (2021)
- Giannios, P., Toutouzas, K.G., Matiatou, M., Stasinou, K., Konstadoulakis, M.M., Zografos, G.C., Moutzouris, K.: Visible to near-infrared refractive properties of freshly-excised human-liver tissues: marking hepatic malignancies. *Sci. Rep.* **6**(1), 1–10 (2016)
- Hatab, N.A., Hsueh, C.H., Gaddis, A.L., Retterer, S.T., Li, J.H., Eres, G., Zhang, Z., Gu, B.: Free-standing optical gold bowtie nanoantenna with variable gap size for enhanced Raman spectroscopy. *Nano Lett.* **10**(12), 4952–4955 (2020)
- Jha, P.K., Shitrit, N., Kim, J., Ren, X., Wang, Y., Zhang, X.: Metasurface-mediated quantum entanglement. *ACS Photonics* **5**(3), 971–976 (2017)
- Jiang, N., Zhuo, X., Wang, J.: Active plasmonics: principles, structures, and applications. *Chem. Rev.* **118**(6), 3054–3099 (2017)
- Johnson, P.B., Christy, R.W.: Optical constants of the noble metals. *Phys. Rev. B* **6**(12), 4370 (1972)
- Kasani, S., Curtin, K., Wu, N.: A review of 2D and 3D plasmonic nanostructure array patterns: fabrication, light management and sensing applications. *Nanophotonics* **8**(12), 2065–2089 (2019)
- King, N.S., Liu, L., Yang, X., Cerjan, B., Everitt, H.O., Nordlander, P., Halas, N.J.: Fano resonant aluminum nanoclusters for plasmonic colorimetric sensing. *ACS Nano* **9**(11), 10628–10636 (2015)
- Lin, G.Q., Yang, H., Deng, Y.D., Wu, D., Zhou, X., Wu, Y., Cao, G., Chen, J., Sun, W., Zhou, R.: Ultra-compact high-sensitivity plasmonic sensor based on Fano resonance with symmetry breaking ring cavity. *Opt. Express* **27**(23), 33359–33368 (2019)
- Liu, K., Xue, X., Sukhotskiy, V., Furlani, E.P.: Optical fano resonance in self-assembled magnetic-plasmonic nanostructures. *J. Phys. Chem. C* **120**(48), 27555–27561 (2016)

- Martinsson, E., Otte, M.A., Shahjamali, M.M., Sepulveda, B., Aili, D.: Substrate effect on the refractive index sensitivity of silver nanoparticles. *J. Phys. Chem. C* **118**(42), 24680–24687 (2014)
- Mejía-Salazar, J.R., Oliveira, O.N., Jr.: Plasmonic biosensing: focus review. *Chem. Rev.* **118**(20), 10617–10625 (2018)
- Nordlander, P.: The ring: a leitmotif in plasmonics. *ACS Nano* **3**(3), 488–492 (2009)
- Panoiu, N.C., Sha, W.E.I., Lei, D.Y., Li, G.C.: Nonlinear optics in plasmonic nanostructures. *J. Opt.* **20**(8), 7–16 (2018)
- Petryayeva, E., Krull, U.J.: Localized surface plasmon resonance: Nanostructures, bioassays and biosensing—A review. *Anal. Chim. Acta* **706**(1), 8–24 (2011)
- Saylan, Y., Akgönüllü, A., Denizli, A.: Plasmonic sensors for monitoring biological and chemical threat agents. *Biosensors* **10**(10), 3–9 (2020)
- Schab, K.R., Outwater, J.M., Young, M.W., Bernhard, J.T.: Eigenvalue crossing avoidance in characteristic modes. *IEEE Trans. Antennas Propag.* **64**(7), 2617–2627 (2016)
- Shrivastav, A.M., Cvelbar, U., Abdulhalim, I.: A comprehensive review on plasmonic-based biosensors used in viral diagnostics. *Commun. Biol.* **4**(1), 1–12 (2021)
- Singh, M., Datta, A.: LSPR excitation on Au nanorings from integrated hybrid plasmonic aperture waveguide and its application in methanol detection in the IR-Band. *IEEE Sens. J.* **19**(15), 6119–6125 (2019)
- Stockman, M.I.: Nanoplasmonic sensing and detection. *Science* **348**(6232), 287–288 (2015)
- Tavakoli, F., Zarrabi, F.B., Saghaei, H.: Modeling and analysis of high-sensitivity refractive index sensors based on plasmonic absorbers with Fano response in the near-infrared spectral region. *Appl. Opt.* **58**(20), 5404–5414 (2019)
- Vardi, Y., Cohen-Hoshen, E., Shalem, G., Bar-Joseph, I.: Fano resonance in an electrically driven plasmonic device. *Nano Lett.* **16**(1), 748–752 (2016)
- Wang, H.: Plasmonic refractive index sensing using strongly coupled metal nanoantennas: nonlocal limitations. *Sci. Rep.* **8**(1), 1–8 (2018)
- Wang, K., Titchener, J.G., Kruk, S.S., Xu, L., Chung, H.P., Parry, M., Kravchenko, I.I., et al.: Quantum metasurface for multiphoton interference and state reconstruction. *Science* **361**(6407), 1104–1108 (2018)
- Wang, M., Zhang, M., Wang, Y., Zhao, R., Yan, S.: Fano resonance in an asymmetric MIM waveguide structure and its application in a refractive index nanosensor. *Sensors* **19**(4), 4–7 (2019)
- Ylä-Oijala, P., Tzarouchis, D.C., Raninen, E., Sihvola, A.: Characteristic mode analysis of plasmonic nanoantennas. *IEEE Trans. Antennas Propag.* **65**(5), 2165–2172 (2017)
- Zarrabi, F.B., Moghadasi, M.N.: Investigated the Fano resonance in the nano ring arrangement. *Optik* **100**(138), 80–86 (2017)
- Zhan, S., Li, H., He, Z., Li, B., Chen, Z., Xu, H.: Sensing analysis based on plasmon induced transparency in nanocavity-coupled waveguide. *Opt. Express* **23**(16), 20313–20320 (2015)
- Zhou, F., Liu, Y., Li, Z.Y., Xia, Y.: Analytical model for optical bistability in nonlinear metal nano-antennae involving Kerr materials. *Opt. Express* **18**(13), 13337–13344 (2010)
- Zhou, J., Liu, S., Qian, H., Li, Y., Luo, H., Wen, S., Zhou, Z., Guo, G., Shi, B., Liu, Z.: Metasurface enabled quantum edge detection. *Sci. Adv.* **6**(51), 2–5 (2020)

Publisher's Note Springer Nature remains neutral with regard to jurisdictional claims in published maps and institutional affiliations.